Chemical Engineering Journal 154 (2009) 295–301

Contents lists available at ScienceDirect

Chemical Engineering Journal

journal homepage: www.elsevier.com/locate/cej

Hydrocracking of long chain linear paraffins

Ilenia Rossetti[a,*], Chiara Gambaro[b], Vincenzo Calemma[b]

[a] Dip. Chimica Fisica ed Elettrochimica, Università degli Studi di Milano, via C. Golgi 19, I-20133 Milano, Italy
[b] ENI S.p.A. R&M Division, via F. Maritano 26, I-20097 S. Donato Milanese, Italy

ARTICLE INFO

Article history:
Received 24 November 2008
Received in revised form 5 March 2009
Accepted 11 March 2009

Keywords:
Hydrocracking
Hydroisomerisation
Upgrading of Fischer–Tropsch waxes

ABSTRACT

The hydrocracking reactivity of two model compounds, namely *n*-$C_{16}H_{34}$ (*n*-C16) and *n*-$C_{28}H_{58}$ (*n*-C28), was investigated on a Pt/SiO_2-Al_2O_3 catalyst. Conversion and products distribution have been determined under a wide range of operating conditions (*i.e.* pressure: 20–80 bar; temperature: 270–330 °C; weight hourly space velocity: 0.33–1.0 h^{-1}; H_2/*n*-paraffin feeding ratio 0.05–0.15 wt/wt). The latter were changed according to a central composite design. The present paper summarises the results obtained on both the model paraffins, depending on the reaction conditions. A first, simple kinetic elaboration is also presented, based on an ideal PFR model and a first order kinetics. The reaction confirmed to be first order with respect to the *n*-paraffin. Experimental data showed that for both *n*-C16 and *n*-C28 conversion was affected by H_2/*n*-paraffin ratio. The change of conversion was explained in terms of vapour liquid equilibrium (VLE), which in turn is affected by the H_2/n-paraffin ratio, so leading to a different vaporisation degree of reactant. In agreement with the VLE data, the effect of H_2/n-paraffin on conversion was lower for *n*-C28. VLE calculations have been carried out to estimate the H_2 partial pressure and degree of vaporisation of the normal paraffin. The reaction order for hydrogen was −1 and −0.5 for *n*-C16 an *n*-C28, respectively. However, in the case of *n*-C16 the data obtained at the lower bound of the pressure range examined displayed an increase of the reaction order. The apparent activation energy was calculated after correction of the contact time taking into account the liquid-vapour equilibrium: similar values have been estimated for *n*-C16 and *n*-C28, *ca.* 32 and 31 kcal/mol, respectively.

1. Introduction

Hydroisomerisation and hydrocracking of alkanes are important refinery processes to obtain high-octane-number reformulated gasoline. Furthermore, waxes, inducing poor cold-flow properties, have to be eliminated through dewaxing and isomerisation of the long-chain *n*-alkanes to moderately branched alkanes, the latter being excellent components for lube oils. The hydroconversion of the synthetic wax produced by the Fischer–Tropsch (FT) process represents a different route for the production of high quality fuels [1]. The FT products are essentially a mixture of linear paraffins spread over a wide range of molecular weight (C_1–C_{70}), due to the polymerisation nature of the reaction. Cobalt catalyzed low temperature FT process is characterised by a products distribution strongly shifted towards heavy components [2,3]. An efficient way to maximize the yields in the middle distillate cut is to subject the FT products to an hydrocracking stage [4,5].

The reaction is efficiently carried out over bi-functional catalysts, consisting of a metal, responsible for hydro-dehydrogenation reactions, dispersed on an oxide support, whose acid sites are responsible of C–C and C–H bonds activation via a carbocationic mechanism. Various metals (e.g. Pt, Ni, Mo) and different acidic supports, such as zeolites, SAPO, sulphated zirconia and amorphous silica–alumina, have been employed [1]. The degree of isomerisation *vs.* cracking can be modulated by proper selection of the acid strength or by taking advantage of the shape selectivity of some zeolite-structured materials. For example, strong acidity (zeolites) favours cracking, while moderate acidity (SAPO) shows higher selectivity for isomerisation [6]. However, catalyst coking and lower selectivity may result from an improper balance between acid sites strength and hydrogenation activity [7]. Some mesoporous materials have been investigated as well, though they seemed suitable for hydroisomerisation more than for cracking, due to milder acidity and lower thermal resistance. With Pt loaded on sulphated zirconia, the cracking/isomerisation ratio rapidly increases with the carbon chain length of the reactant molecule [8].

As for the metallic function, the easier the hydrogenation step, the lower is the carbocation lifetime, with subsequent lower probability of secondary cracking events [1]: for the hydrocracking of "clean" feedstocks (free of sulphur, metals and oxygenated compounds) noble metals are suitable hydrogenating active sites, being

* Corresponding author. Tel.: +39 02 50314059; fax: +39 02 50314300.
E-mail address: ilenia.rossetti@unimi.it (I. Rossetti).

1385-8947/$ – see front matter © 2009 Elsevier B.V. All rights reserved.
doi:10.1016/j.cej.2009.03.018

Table 1
Parameters settings for each level of the factorial plan.

	n-C16				*n*-C28			
Level #	T (°C)	P (bar)	WHSV (h^{-1})	H_2/*n*-paraffin (wt/wt)	T (°C)	P (bar)	WHSV (h^{-1})	H_2/*n*-paraffin (wt/wt)
−2	290	20	1,0	0.050	285	20	1.0	0.050
−1	300	35	1,5	0.075	295	35	1.5	0.075
0	310	50	2,0	0.100	305	50	2.0	0.100
1	320	65	2,5	0.125	315	65	2.5	0.125
2	330	80	3,0	0.150	325	80	3.0	0.150

very active; otherwise, also non-noble transition metals, such as Ni, Co, Mo and W, are used [6].

The hydrocracking mechanism can be schematically represented as a series of isomerisation and cracking steps: the *n*-paraffin in the feed is isomerised to the corresponding mono-branched paraffin, which is in turn converted to the di-branched paraffin and so on; the multi-branched paraffins are then cracked to lighter products [9].

The kinetics of the reaction has been modelled following different approaches. A fundamental one is based on the Langmuir–Hinshelwood–Hougen–Watson approach (LHHW), which decomposes the reaction in a series of elementary steps, to be modelled with proper rate expressions and subsequently lumped to describe the products distribution [10,11]. A different approach is represented by the "single event kinetics" (SE): a network of elementary reactions is designed taking into account the formation of each single component of the product mixture [12–14]. The SE kinetics is based on the "chemical knowledge" of each elementary step involved in the reaction; thus rate parameters have a general meaning and can be applied to different feeds [15]. On the other hand, due to the complicated network of rate expressions, the SE approach is best applied to model compounds rather than to complex mixtures, such as FT waxes, due to extremely increasing calculation time, although efforts have been made to simplify some points [14] and to extrapolate the results to real mixtures. The kinetic description of the hydrocracking of complex mixtures has been generally achieved, at least up to now, by means of lumped models [16–20].

According to our knowledge, in literature there are very few kinetic studies carried out on single components of relatively high molecular weight [9,21]. Such data are indeed needed to better support the interpretation of the behaviour of complex mixtures. The aim of the present work was then to collect kinetic data for the hydrocracking of two paraffins of relatively high molecular weight, namely *n*-$C_{16}H_{34}$ (*n*-C16) and *n*-$C_{28}H_{58}$ (*n*-C28). The effect of four different parameters, *i.e.* temperature, pressure, H_2/*n*-paraffin ratio and contact time, on conversion and selectivity has been checked following a factorial experimental plan. A first simple kinetic analysis is also presented.

2. Experimental

2.1. Set up of the apparatus

The experimental apparatus was made up of a down-flow continuous Incoloy 800 tubular reactor (400 mm in length, 10.3 mm internal diameter), surrounded by two heavy AISI 316 hemicylindrical blocks and heated by an electric furnace, controlled by an Eurotherm (mod. 822, coupled to a mod. 425S power unit) TIC. The paraffins, stored in a heated tank, so to keep them in liquid form, were fed to the reactor by means of a heated syringe pump (Isco, mod. 314). H_2 flow rate was regulated by means of a Brooks (mod. 5850S) mass flow meter, governed by a control unit (Brooks, mod.154). A pressurised storage tank at the exit of the reactor was employed for the collection of liquid products, whereas the flow rate of the gaseous fraction was measured by a volumetric wet-test meter (Elster Handel, ser. 63004054). The reaction pressure was regulated by means of a home-made PTFE-membrane relief valve, pressurised with nitrogen at the desired value. A high-precision manometer, a bursting-disc safety device and heating devices on the whole feeding and reaction lines completed the apparatus.

Kinetic data have been collected on *ca.* 5 g of a Pt/amorphous SiO_2-Al_2O_3 catalyst in 20–45 mesh particle size (bed volume *ca.* 10 cm^3 and bed length *ca.* 12 cm, fitting the isothermal central part of the furnace). Catalyst wetting has been checked for this particle size and under the selected operating conditions according to the Gierman and Harmsen criteria as suggested in [22]. The void part of the reactor, above and below the catalyst bed, was filled with quartz beads (10–20 mesh), previously washed with diluted HCl and calcined at 450 °C in air. Catalyst activation was carried out by heating up to 400 °C in flowing H_2.

Catalytic activity has been monitored for 5 days until the attainment of steady-state conditions for every new feed. After completion of the kinetic experimentation on *n*-C16 the whole apparatus was carefully washed at first with *n*-C7, then with *n*-C28, and again the activity was monitored until the attainment of steady state conversion before starting the collection of the data on *n*-C28.

2.2. Planning of experimental tests

Kinetic data have been collected using a central composite design approach [23], based on four variables: temperature (T), pressure (P), weight hourly space velocity (WHSV), H_2/*n*-paraffin (wt/wt) and for every set of four parameters conversion of the reactant (*n*-C16 or *n*-C28) and selectivity to the various products or lumps have been determined.

The central run conditions (level [0 0 0 0]) have been set in order to attain *ca.* 50% conversion of the *n*-paraffin. The experiments have been made on two levels [+1 −1], plus for every factor four further levels were added [+2 +1 −1 −2] and central runs were periodically and frequently repeated. The complete experimental plan for each feed included a first set of 25 runs, made in a random sequence, plus various additional tests to address specific topics and for reproducibility checking for a total of *ca.* 50 runs. The values of the four factors corresponding to each level are listed in Table 1. After the completion of kinetic data measurements on *n*-C28, some tests have been added for *n*-C16, showing reproducibility with previous runs and excluding any severe deactivation of the catalyst.

2.3. Analysis of the reaction products

For every run a one hour-on-stream time was left to attain steady state conditions. This time interval showed sufficient for this purpose during the preliminary tests carried out for setting up the apparatus. Then, a 1 h run started for each test, during which the liquid products were collected in the pressurised tank and subsequently analysed, while effluent gas analysis was carried out at least twice during each run. Aliquots of the collected liquid products were then dissolved in CS_2 and analysed.

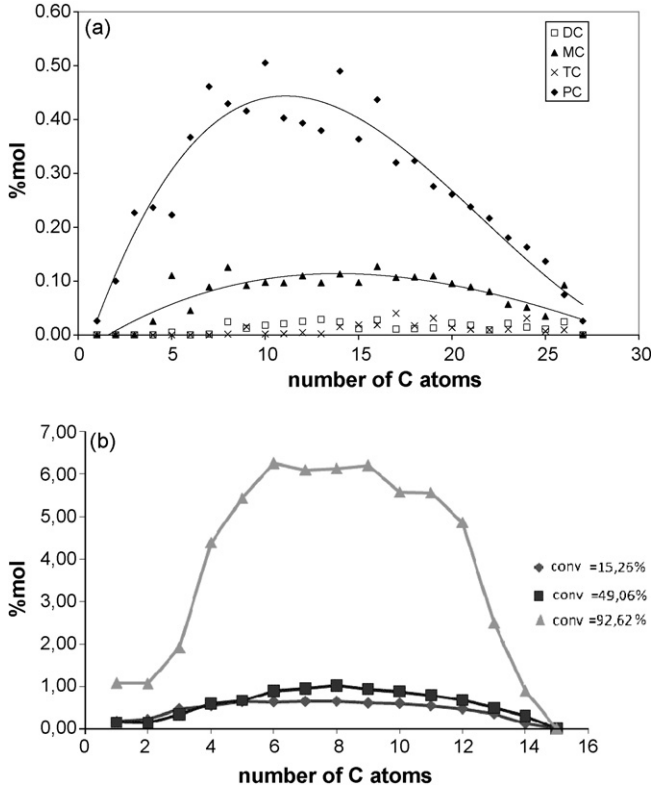

Fig. 1. Typical cracking products distribution for central runs when feeding *n*-C28 (*ca.* 50% conversion). PC = linear, MC = mono-branched (methyl- + ethyl-substituted), DC = di-methyl substituted, TC = tri-methyl substituted paraffins.

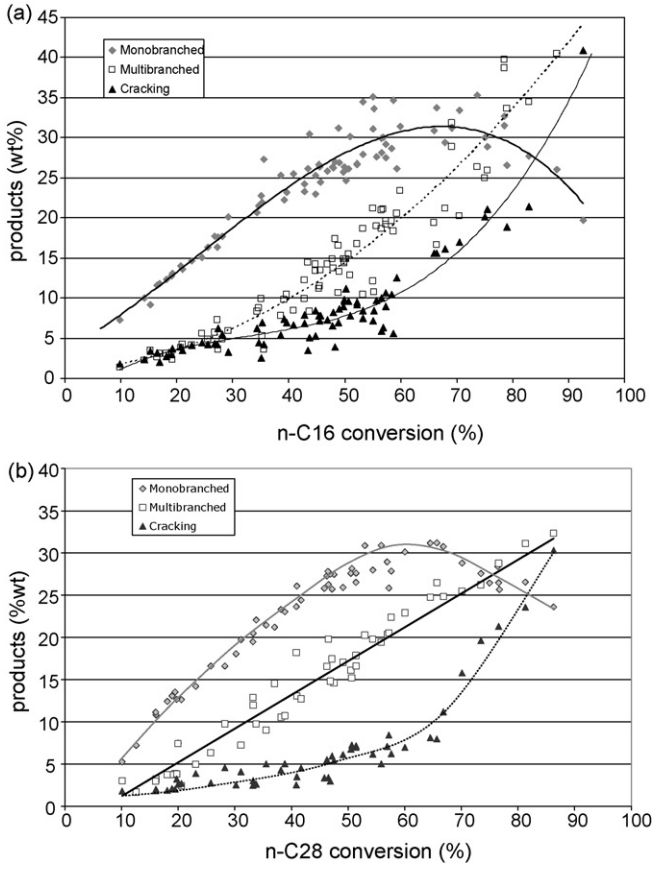

Fig. 2. Product distribution (%wt in the collected liquid and gas phases) as a function of conversion for (a) *n*-C16 and (b) *n*-C28. "Mono-" and "multi-branched" products refer to the feed isomerisation only, "cracking" products were calculated as $C_1 - C_{n-1}$ lump (linear + branched isomers).

The analysis of both liquid and gaseous products has been made off-line by means of a properly calibrated Agilent 6890 gas chromatograph, equipped with flame ionisation (FID) and hot-wire (HWD) detectors and with HP-5 and PoraPlot Q columns for liquid and gas analysis, respectively, with H_2 as carrier gas. Due to the relatively poor resolution for different isomers, the results have been lumped as linear (PC), mono-methyl substituted (MC), di-methyl substituted (DC), tri-methyl substituted (TC) and ethyl-substituted (EC) paraffins, as exemplified in Fig. 1.

3. Results and discussion

3.1. Effect of the main operating parameters on activity

A typical distribution of hydrocracking products as a function of chain length is presented in Fig. 1a, which reports the average results of the central runs carried out on *n*-C28. The cracking products consist mainly of linear paraffins and mono-branched compounds, followed in descending order by di-, tri-branched alkanes. Moreover, experimental results (not shown for the sake of brevity) display that the molar ratio between iso- and *n*-paraffins increases with conversion, at constant temperature, in a rather exponential way, due to consecutive isomerisation reactions [24]. Monobranched isomers are essentially a mixture of monomethyl (predominant) and ethyl-paraffins. Formation of methyl branching can be readily explained according to the protonated cyclopropane mechanism (PCP) [25]. Based on the same reaction mechanism, ethyl-substituted isomers are less favoured, due to the lower stability of the cyclobutane intermediate [26].

A flat products distribution was observed at low conversion, which evolves to a bell-shaped curve at high conversion, as reported in Fig. 1b for *n*-C16. A shift towards low-molecular weight products was observed particularly at high conversion levels, where the subsequent cracking of first formed products is quantitatively significant. As previously reported in literature for lower molecular weight normal paraffins, regardless the operating conditions [27,28] the isomer and cracking yields, reported in Fig. 2a and b, are a unique function of the total conversion, thus indicating a similar activation energy of the hydroisomerisation and hydrocracking reactions. Furthermore, the evolution of both systems is in agreement with a reaction pathway where the conversion of *n*-alkane occurs through a series of consecutive reactions: the *n*-alkane is first isomerised into mono-branched isomers, which undergo subsequent isomerisation steps and cracking reactions.

The effect of the operating conditions, temperature, pressure, H_2/*n*-paraffin ratio and WHSV, on the conversion of the two model compounds (*n*-C16 and *n*-C28) is reported in Fig. 3a–d. Fig. 3a depicts the dependence of conversion on temperature for both reactants. Conversion always increased with temperature, as expected, due to kinetic reasons. The conversion of *n*-C28 was always higher than that of *n*-C16, this can be accounted for by the fact that the reactivity is expected to be proportional to the number of secondary carbon atoms per molecule or, as proposed by Sie, to C_{n-6} and C_{n-4} for hydrocracking and hydroisomerisation respectively [29]. However, as reported in several works [30,31], the higher reactivity of heavier *n*-paraffins can be also ascribed to their stronger physisorption, which lead to a higher density on the catalyst surface and consequently to higher reaction rates.

Fig. 3b reports the effect of total pressure on conversion. For both feedstocks conversion decreased with increasing pressure. The negative dependence of normal alkane conversion on hydrogen can be explained in terms of a bi-functional mechanism where

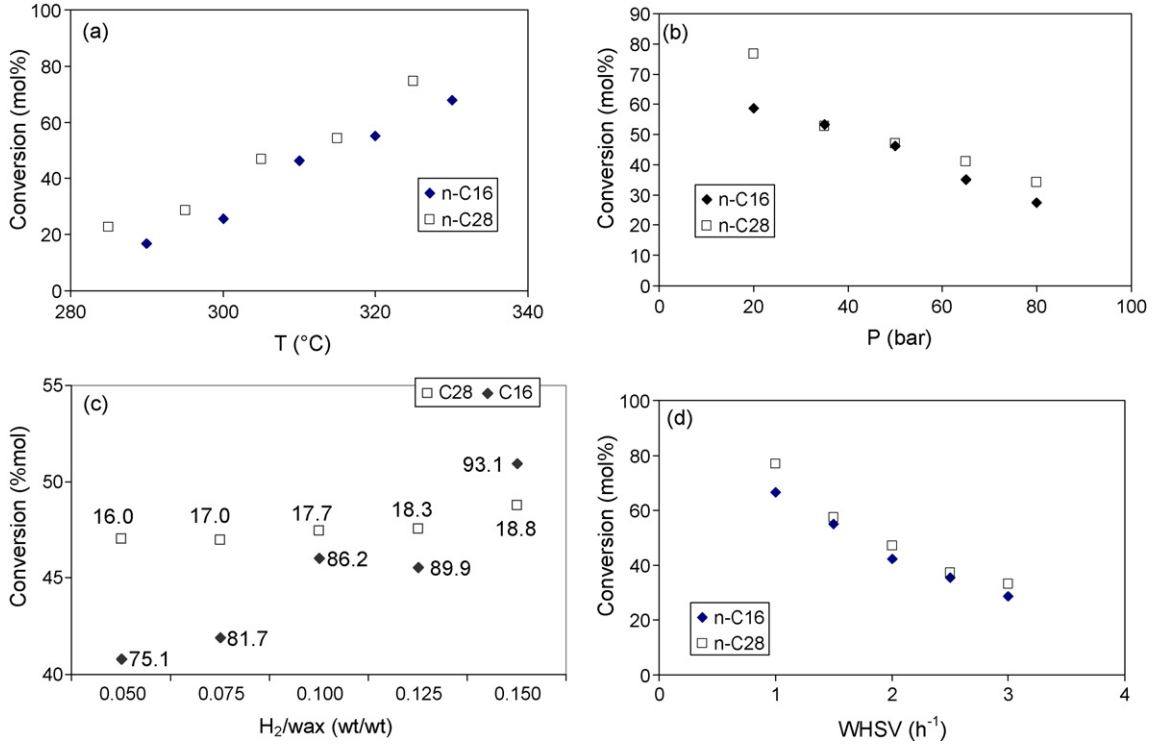

Fig. 3. Dependence of conversion of *n*-C16 and *n*-C28 on the operating parameters: (a) temperature, (b) total pressure, (c) H_2/*n*-paraffin ratio and (d) space velocity. The numbers on Fig. 2c represent the percentage of evaporated wax.

the first step is the formation of olefins at the metal site, subsequent formation of secondary carbenium at the acidic site and then the various steps leading to the final products [11]. In this scheme the rate determining step is the rearrangement of the secondary carbenium while the other reactions are considered to be in quasi equilibrium conditions, hence an increase of hydrogen pressure will lead to lower steady state concentrations of *n*-alkenes and consequently of secondary carbenium ions, which results in a decrement of the limiting step rate [32,33]. This conversion *vs.* pressure trend also confirms that the catalyst is operating under "ideal" conditions, *i.e.* it is possible to consider the hydro/dehydrogenation steps in quasi-equilibrium [7,34].

Feed conversion *vs.* H_2/*n*-paraffin weight ratio is reported in Fig. 3c. Higher H_2/*n*-paraffin inlet ratios led to an increase in the paraffin conversion. The effect is much more pronounced in the case of *n*-C16 than for *n*-C28. Notably, the reaction mechanism foresees a decrease in the reaction rate with the increase of the H_2/*n*-paraffin ratio rather than an increase as experimentally observed [12]:

$$r = k_{iso} c_{tot} \frac{K_{DH} K_{PROT} (P_{nP}/P_{H_2})}{((1 + K_{LP} P_{nP})/c_{ps} K_{LP}) + K_{DH} K_{PROT} (P_{nP}/P_{H_2})} \quad (1)$$

where k_{iso} is the kinetic constant for the isomerisation reaction, K_{DH} and K_{PROT} are the hydro-dehydrogenation and protonation equilibrium constants, K_{LP} is the Langmuir physisorption equilibrium constant for the *n*-paraffin, c_{tot} is the concentration of acid sites, c_{ps} is the maximum concentration of paraffin in the catalyst pores, P_i is the partial pressure of the reactant (H_2 or paraffin[1]). The equation refers to the case of low conversion, where the iso-paraffin concentration is low. The promoting effect of the H_2/wax ratio on conversion should rather be explained considering the role of this parameter on vapour-liquid equilibrium (VLE) [36]. Depending on the reaction conditions and paraffin used during the tests, a fraction of the normal paraffin evaporates from the liquid to the vapour phase. The "degree of evaporation" of the hydrocarbon changes with the H_2/wax ratio, as demonstrated by calculations carried out with a routine based on SRK equation of state, considered one of the most suitable for this problem [37,38], whose results are reported in Fig. 3c. The same calculation showed that only a small fraction of H_2 (ca. 0.5 wt% with respect to the H_2 fed, in first approximation considered negligible) was dissolved in liquid phase in the case of *n*-C16 under the conditions of the central run, taken as reference. We observed that in both cases the paraffin fraction in the vapour phase increases along with the increase of the H_2/*n*-paraffin ratio, but remarkable quantitative differences exist as for the entity of the phenomenon. In the case of *n*-C16 the fraction in vapour phase at the reactor inlet ranges between 75.1 and 93.1%, whereas in the case of *n*-C28, its percentage in gas phase is much lower and displays a lower variation. In these circumstances, the increase in conversion with the rise of H_2/*n*-paraffin ratio can be rather ascribed to the change in VLE, leading to higher fraction of reactant and products in the gas phase. We can assume that the reaction occurs in an ideal trickle flow regime and that the reactive part is in liquid phase, in contact with the catalyst, the gas phase simply being in equilibrium with the liquid one. On this basis, the conversion would in first approximation be a function of the space velocity of the liquid phase, rather than of the overall space velocity at the rector inlet. The equation defining the relationship between conversion and residence time for a first order reaction: $y_f = 1 - e^{-k/WHSV}$. The plot of $\ln(1-y_f)$ *vs.* 1/WHSV (or τ) should be a straight line, whose slope is the kinetic constant *k*. The latter is only affected by temperature and should remain constant when other operating conditions are changed. In the case of *n*-C16, different values of *k* can be estimated changing the H_2/*n*-paraffin ratio when the inlet WHSV = 2 h^{-1} is considered (see Fig. 4a). This happens because a significant amount of the reactant evaporates: if the real space velocity of the liquid

[1] In this specific case, due to their high molecular weight, the paraffins are not in gas phase, so the notation P_{n-P} is not completely correct: a more reliable way to write this rate expression for heavy hydrocarbons is to use fugacity [35].

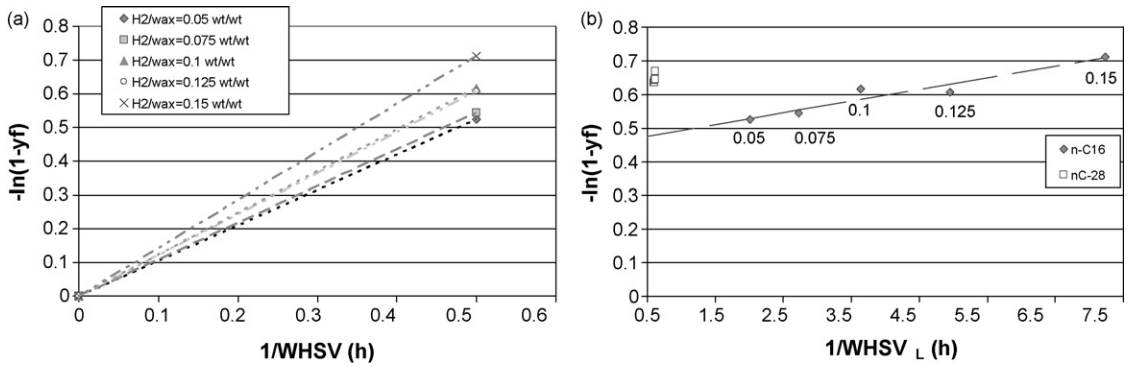

Fig. 4. Conversion as a function of (a) the WHSV for *n*-C16 and (b) the $WHSV_L$, of the liquid phase, for *n*-C16 and *n*-C28. The numbers on (b) represent the experimental H_2/*n*-paraffin ratio.

phase, $WHSV_L = (1-f)\cdot WHSV$ (where *f* is the degree of evaporation) is considered, then the points at different H_2/*n*-paraffin ratios are aligned on the same trace, as shown in Fig. 4b. The minimum *x*-value that the plot can reach is $\tau_L = 0.5$ h, that is the case in which the paraffin remains all in liquid phase and the space velocity of the liquid phase coincides with the inlet WHSV. The point where the plot crosses the line $\tau_L = 0.5$ h gives the conversion when no evaporation occurs, and is related to the intrinsic reactivity of the liquid phase.

Finally, the effect of WHSV on conversion is shown in Fig. 3d. As expected, conversion decreased with increasing space velocity, *i.e.* with decreasing contact time. The cracking products concentration increased rather monotonously with conversion, as the multi-branched C16 or C28 isomers. By contrast, the mono-substituted isomers concentration increased with conversion and contact time, decreasing at the lowest value of WHSV, predominantly due to transformation into cracking products. It is worth noticing that the products distribution shifted towards lighter products with increasing contact time, due to secondary cracking for both feedstocks.

Summarising, the dependence of conversion on the above reported parameters can be sketched as follows: (i) the higher the conversion, the lower is the amount of intermediate molecular weight products, indicating the presence of consecutive cracking reactions; (ii) a temperature increase brings about an increase of conversion, due to kinetic reasons; (iii) conversion decreases with increasing pressure, due to the increase of hydrogen partial pressure; (iv) an increase of WHSV means a decrease of contact time and has a negative effect on conversion; (v) the H_2/*n*-paraffin ratio affects the liquid-vapour equilibrium of the reacting mixture. A high H_2/*n*-paraffin ratio (*i.e.* higher hydrogen concentration) increases the degree of vaporisation of light species and causes a higher concentration of the heavier species in the liquid phase. The latter being more reactive, the conversion increases. This effect was much more evident for *n*-C16 than for *n*-C28.

3.2. Simplified kinetic analysis

A simplified approach was followed to estimate the reaction order with respect to the paraffin (*n*-C16 or *n*-C28) and H_2 and to calculate the apparent activation energy. For this purpose, the data were analysed considering an ideal plug-flow reactor and a first order rate expression with respect to the paraffin. In order to check the reliability of the latter hypothesis, at first the hydrogen partial pressure was assumed constant, H_2 conversion being usually lower than 10%. With such constraints, the following relationship holds between conversion and contact time:

$$-\ln(1-y_f) = k\tau \quad (2)$$

y_f being conversion, *k* the kinetic constant and τ the contact time. If the hypothesis of first order kinetics for the paraffin is correct, by plotting $Y = -\ln(1-y_f)$ *vs.* τ, a straight line, with zero intercept and slope *k* should be obtained.

Under reaction conditions the feed is subjected to vapour-liquid equilibrium, the contact time in the simplified model should actually be that of the liquid phase covering the catalyst particle and considered as the reactive portion of the paraffin, the contribution to reactivity of the gas phase being less important (*vide supra*). The tests performed at different space velocities were used for this purpose and the results are plotted in Fig. 5: the simplified model seems to work well, since good correlations have been obtained for both the paraffins.

This approach was applied to the data collected at different temperatures: the estimated kinetic constants were used to calculate the apparent activation energies for the two reactants by means of the Arrhenius equation: regression of the results gave a value of 32.1 kcal/mol for *n*-C16 and 30.8 kcal/mol for *n*-C28. These are roughly in line with literature data based on lumped kinetic models, with a slight overestimation in some cases [9,39,40] and support the observed higher reactivity of *n*-C28 with respect to n-C16.

3.3. Reaction order with respect to H_2

The reaction order with respect to H_2 was evaluated introducing a power law rate expression and, as a first approximation, neglecting the H_2 amount dissolved in liquid phase. Furthermore, p_{H2} has been calculated by subtraction of the paraffin partial pressure (calculated on the basis of VLE) from the total pressure. The different composition along the reactor has not been taken into account. Hence, the following rate equation was used, considering the partial

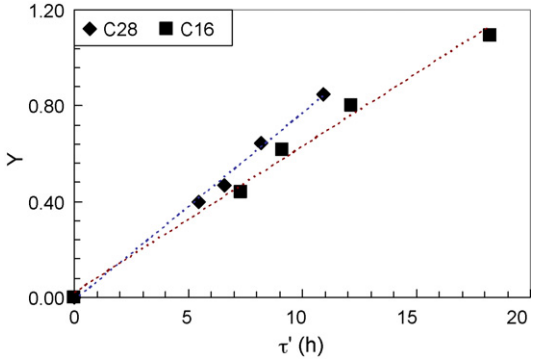

Fig. 5. First order reaction plot for *n*-C16 and *n*-C28 conversion. ($Y = -\ln(1-y_f)$). Contact time (τ') refers to the paraffin in liquid phase.

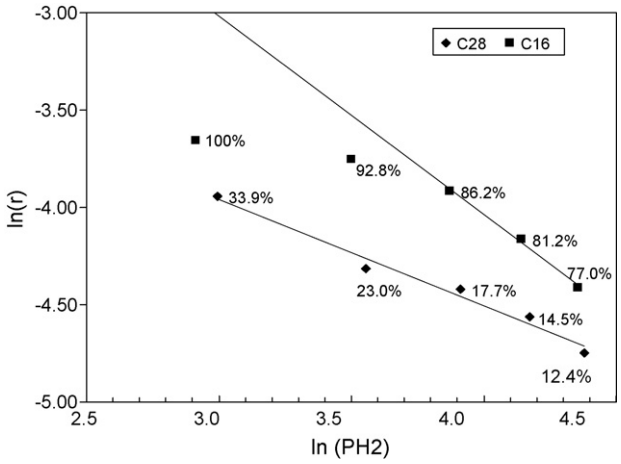

Fig. 6. Reaction order with respect to H_2. The numbers on the plot represent the degree of evaporation of the wax.

pressure of the n-paraffin as a constant:

$$\text{Reaction rate (mol/h)} = k' p_{H_2}^{\alpha} \quad (3)$$

Linearization has been achieved by a bi-logarithmic plot of the reaction rate against hydrogen pressure: the slope of the regression line corresponds to the H_2 reaction order, α.

Results are reported in Fig. 6: a linear plot was obtained for the case of n-C28, with a slope of −0.55. Notably, H_2 partial pressure is close to the total pressure, in line with a low volatility of the paraffin under reaction conditions. By contrast, n-C16 partial pressure was not negligible, in particular at the lowest pressures. Even if the correction due to VLE was applied, a non-linear pattern has been obtained with *n*-C16, as depicted in Fig. 6. Then only the three points at higher pressure have been taken into account for regression and a reaction order for H_2 of −1.0 was estimated for *n*-C16. A negative reaction order was indeed expected, due to the first dehydrogenation step of the reaction [10,41]. However, so different values for the two paraffins seem surprising, as well as the singular pattern obtained with *n*-C16.

Ribeiro et al. [40] proposed an explanation for the fractional H_2 reaction order, in light of the bi-functional mechanism usually assumed. Removing the adsorption–desorption equilibrium expression from equation (1), it can be rearranged as follows:

$$r = k_{iso} c_{tot} \frac{K_1 K_2 c_{nP^*}}{P_{H_2} + K_1 K_2 c_{nP^*}} \quad (4)$$

where c_{nP^*} is the concentration of the adsorbed *n*-paraffin, k_{iso} the kinetic constant of isomerisation, K_1 the equilibrium constant of dehydrogenation, K_2 that of carbenium ion formation, while c_{tot} is given by the product of K_1,K_2 and the concentration of acid sites. Looking at Eq. (4), if the product $K_1 K_2 c_{nP^*}$ is negligible with respect to the H_2 partial pressure, the reaction order with respect to hydrogen is actually −1, as in the case of light paraffins (C6 [40], C10 [10] and present data on *n*-C16), otherwise a fractional reaction order is found, as in our case with *n*-C28. In fact, K_1 and K_2 increase with the chain length for entropic reasons, as proposed by de Gauw et al. [42]. In addition adsorption phenomena increase with chain length. As a consequence, the product $K_1 K_2 c_{nP^*}$ is never negligible with respect to P_{H2} in the case of *n*-C28. Otherwise, in the case of *n*-C16 the trend observed witnesses the transition between two regimes: from high hydrogen pressure values, where the term $K_1 K_2 c_{nP^*}$ is negligible with respect to the H_2 partial pressure, to low values of the latter where the term $K_1 K_2 c_{nP^*}$ is no more negligible, thus leading to a fractional order. A factor which may contribute in this direction is the higher degree of evaporation at low pressure, as shown in Fig. 6. Higher evaporation degrees correspond to a higher paraffin partial pressures and therefore to lower H_2 partial pressures: under these conditions, the product $K_1 K_2 c_{nP^*}$ is not negligible and a fractional reaction order towards H_2 is obtained.

4. Conclusions

A set of kinetic data for the hydrocracking reaction has been collected on *n*-$C_{16}H_{34}$ and *n*-$C_{28}H_{58}$. The effect of the main reaction parameters (temperature, pressure, H_2/wax ratio and space velocity) on conversion and products distribution has been investigated. Conversion of both normal paraffins is affected by the H_2/*n*-paraffin ratio indicating that a significant role is played by the VLE. In agreement with the VLE data, the effect of H_2/*n*-paraffin ratio on conversion is higher in the case of *n*-C16, which displays a wider change of vaporization degree. Both *n*-C16 and *n*-C28 showed a first reaction order with respect to the *n*-paraffin. Reaction order with respect to hydrogen resulted to be *ca.* −1 for *n*-C16 and *ca.* −0.5 for *n*-C28. However, different regimes can be envisaged in the case of *n*-C16, depending on hydrogen partial pressure. Tentatively, we suggest that the fractional order for hydrogen observed for *n*-C28 is due to a term in the rate equation containing the constant of protonation and dehydrogenation, which is not negligible. Within the same line of reasoning one can explain the change of reaction order with respect to hydrogen displayed by the *n*-C16. In agreement with the values generally reported in literature [9,10] the apparent activation energies were *ca.* 32.1 and 30.8 kcal/mol, for *n*-C16 and *n*-C28 respectively.

Acknowledgments

The valuable help of A. Landoni, M. Bos and B. Cortese is gratefully acknowledged.

References

[1] V.M. Akhmedov, S.H. Al-Khowaiter, Catal. Rev. 49 (2007) 33.
[2] M.E. Dry, Catal. Today 71 (2002) 227.
[3] R.L. Espinoza, A.P. Steynberg, B. Jager, A.C. Vosloo, Appl. Catal. A: Gen. 186 (1999) 13.
[4] M.J. Murphy, J.D. Taylor, R.I. Mc Cormic, Compendium of Experimental Cetane Number Data, NREL/SR-540-36805 (2004).
[5] D.R. Lide (Ed.), Handbook of Chemistry and Physics, 85th Ed., CRC Press, Boca Raton, Florida, 2004–2005.
[6] H. Deldari, Appl. Catal. A:Gen. 293 (2005) 1.
[7] J.W. Thybaut, C.S. Laxmi Narasimhan, J.F. Denayer, G.V. Baron, P.A. Jacobs, J.A. Martens, G.B. Marin, Ind. Eng. Chem. Res. 44 (2005) 5159.
[8] E. Iglesia, S.L. Soled, G.M. Kramer, J. Catal. 144 (1993) 238.
[9] V. Calemma, S. Peratello, C. Perego, Appl. Catal. A 190 (2000) 207.
[10] M. Steijns, G.F. Froment, Ind. Eng. Chem. Prod. Res. Dev. 20 (1981) 660.
[11] M.A. Baltanas, H. Vansina, G.F. Froment, Ind. Eng. Chem. Prod. Res. Dev. 22 (1983) 531.
[12] G.F. Froment, Catal. Today 1 (1987) 455.
[13] G.F. Froment, Catal. Rev. Sci. Eng. 47 (2005) 83.
[14] E. Valéry, D. Guillaume, K. Surla, P. Galtier, J. Verstraete, D. Schweich, Ind. Eng. Chem. Res. 46 (2007) 4755.
[15] G.D. Svoboda, E. Vynckier, B. Debrabandere, G.F. Froment, Ind. Eng. Chem. Res. 34 (1995) 3793.
[16] N. Bhutani, A.K. Ray, G.P. Rangaiah, Ind. Eng. Chem. Res. 45 (2006) 1354.
[17] S. Sànchez, J. Ancheyta, Energy Fuels 21 (2007) 653.
[18] L. Pellegrini, S. Bonomi, S. Gamba, V. Calemma, D. Molinari, Chem. Eng. Sci. 62 (2007) 5013.
[19] P. Castaño, J.M. Arandes, B. Pawelec, M. Olazar, J. Bilbao, Ind. Eng. Chem. Res. 47 (2008) 1043.
[20] P. Balasubramanian, S. Pushpavanam, Fuel 87 (2008) 1660.
[21] V. Calemma, S. Peratello, F. Stroppa, R. Giardino, C. Perego, Ind. Eng. Chem. Res. 43 (2004) 934.
[22] L.F. Ramìrez, J. Escobar, E. Galvàn, H. Vaca, F.R. Murrieta, M.R.S. Luna, Petroleum Sci. Tech. 22 (2004) 157.
[23] K. Hinkelmann, O. Kempthorne, Design and Analysis Of Experiments, Vol. 2: Advanced Experimental Design, Wiley, 2005.
[24] T.D. Pope, J.F. Kriz, M. Stanciulescu, J. Monnier, Appl. Catal. A 233 (2002) 45.
[25] S.T. Sie, Ind Eng. Chem. Res. 31 (1992) 1881.
[26] C. Marcilly, Catalyse acido-basique. Application au raffinage et à la pétrochimie, Editions Technip 2003, vol. 1, chapter 3, p. 168.

[27] M. Steijns, G.F. Froment, P. Jacobs, J. Uytterhoeven, J. Weitkamp, Ind. Eng. Chem. Prod. Res. Dev. 20 (1981) 654.
[28] J. Weitkamp, A. Jacobs, J.A. Martens, Appl. Catal. 8 (1983) 123.
[29] S.T. Sie, Ind Eng. Chem. Res. 32 (1993) 403.
[30] J.F.M. Denayer, B. De Jonckheere, M. Hioch, G.B. Marin, G. Vanbutsele, J.A. Martens, G.V. Baron, J. Catal. 210 (2002) 445.
[31] J.F.M. Denayer, R.A. Ocakoglu, W. Huybrechts, B. De Jonckheere, P. Jacobs, S. Calero, R. Krishna, B. Smit, G.V. Baron, J.A. Martens, J. Catal. 220 (2003) 66.
[32] M.A. Baltanas, K.K. van Raemdonck, G.F. Froment, S.R. Mohedas, Ind. Eng. Chem. Res. 28 (1989) 899.
[33] H. Kumar, G.F. Froment, Ind. Eng. Chem. Res. 46 (2007) 4075.
[34] J.W. Thybaut, C.S. Laxmi Narasimhan, G.B. Marin, Catal. Today 111 (2006) 94.
[35] L.A. Pellegrini, S. Gamba, V. Calemma, S. Bonomi, Chem. Eng. Sci. 63 (2008) 4285.
[36] V. Calemma, S. Correra, C. Perego, P. Pollesel, L. Pellegrini, Catal. Today 106 (2005) 282.
[37] J.V. Sengers, R.F. Kayser, C.J. Peters, H.J. White (Eds.), Equations of State for Fluids and Fluid Mixtures, Elsevier, Amsterdam, 2000.
[38] J.O. Valderrama, Ind. Eng. Chem. Res. 42 (2003) 1603.
[39] B. Debrabandere, G.F. Froment Stud.Surf.Sci.Catal. 106 (1997) 379.
[40] F. Ribeiro, C. Marcilly, M. Guisnet, J. Catal. 78 (1982) 267.
[41] V.M. Akhmedov, K.J. Klabunde, J. Mol. Catal. 45 (1988) 193.
[42] F.J.M.M. de Gauw, J. van Grondelle, R.A. van Santen, J. Catal. 206 (2002) 295.